Scientific Reports

https://doi.org/10.1038/s41598-026-59600-w

Article in Press

Two-in-one terahertz metasurface: a widely adjustable narrowband perfect absorber and a highly sensitive biosensor

Received: 22 January 2026

Accepted: 22 June 2026

Published online: 03 July 2026

Cite this article as: Hosseini S.M. & Jahangiri F. Two-in-one terahertz metasurface: a widely adjustable narrowband perfect absorber and a highly sensitive biosensor. *Sci Rep* (2026). https://doi.org/10.1038/s41598-026-59600-w

Seyyedeh Maryam Hosseini & Fazel Jahangiri

Two-in-One Terahertz Metasurface: A Widely Adjustable Narrowband Perfect Absorber and a Highly Sensitive Biosensor

Seyyedeh Maryam Hosseini, Fazel Jahangiri*
Laser and Plasma Research Institute, Shahid Beheshti University, Tehran, Iran
* f_jahangiri@sbu.ac.ir
https://orcid.org/0000-0001-6550-3723
https://orcid.org/0000-0002-7931-7320

Abstract:

A dual-function terahertz metasurface is **designed under idealized (noise-free, lossless) simulation conditions** based on a copper-based resonator. The meta-structure serves not only as a perfect narrowband absorber but also as a highly sensitive refractive index sensor for analytes. The proposed meta-structure features a **compact, ultrathin**, simple, single-material design based on a periodic array of circular rings and disks. A near-perfect absorption of 99.99% is demonstrated at the resonant frequency of 0.8 THz, which can be **configured** over the span of 0.53–1.47 THz via geometric parameters and dielectric permittivity adjustments. The meta-absorber design is confirmed to be polarization-insensitive and also wide-angle, preserving the absorption $>$ 90% for a wide range of incident angles up to 45° (TE) and 75° (TM). The meta-absorber functions as a high-performance dual-mode metasensor, simultaneously measuring both the analyte's thickness and refractive index. Under TE polarization, it achieves a refractive index sensitivity of 0.173 THz/RIU (with a FOM of 3.47 RIU^{-1} and a Q-factor of 12.76) for thick analytes, while also providing a thickness sensitivity of 14 GHz/μm for ultrathin analytes. This study presents a cost-effective and high-performance platform for terahertz sensing applications. Its straightforward fabrication can render it as a competitive alternative to more complex metasurface designs.

1. Introduction

Perfect absorbers play a crucial role in achieving ultrasensitive detection because they can entirely trap electromagnetic energy, creating strong local fields necessary for examining small material changes. This capability is applicable in the visible [1], infrared [2], and terahertz (THz) [3, 4] spectral ranges. The THz regime enables the non-destructive, label-free analysis of materials by probing their unique low-energy molecular vibrations and rotations [5]. This ability supports high-specific sensing by identifying minute changes in the refractive index of key analytes, including biomolecules such as DNA [6] and RNA [7].

Metasurfaces, a class of subwavelength-thick planar meta-atoms, are architected for a dual role, i.e., a resonant absorber employed as a highly sensitive sensor [8, 9]. THz metasurfaces provide a compelling alternative to conventional methods such as fluorescent labeling [10] and radioisotope-based methods [11] for advanced biosensing applications. These surfaces exhibit attributes such as strong field confinement, tunable resonances, and enhanced light–matter interactions. Numerous studies have demonstrated their potential as compact, cost-effective, and high-performance biosensors capable of detecting minute chemical and biological analytes [12-21]. In metasurface-based resonant cavities, key performance parameters—including resonance frequency, quality factor (Q-factor), and electric field confinement—are primarily dictated by the geometry, composition, and dimensions of the meta-atom unit cell, as well as the surrounding medium [22]. Metallic metasurfaces typically employ unit cells composed of common or noble metals such as gold (Au) [23], aluminum (Al) [24], silver (Ag) [25], and copper (Cu) [26]. These metals facilitate pronounced field enhancement in air [27], where analyte interaction occurs, thereby enabling high sensitivity [8, 28]. Nonetheless, their inherent ohmic losses significantly degrade the Q-factor [22].

Among the various metasurface configurations, metasurface perfect absorbers (MPAs) have emerged as promising platforms for THz biosensing [8, 29-39]. These structures achieve near-unity absorption by simultaneously suppressing reflection and transmission via impedance matching to free space and through the incorporation of a metallic ground plane, respectively. This dual mechanism enables efficient confinement of incident THz radiation within the metasurface, thereby amplifying its interaction with surface-bound analytes and enhancing sensing performance. Pioneering work in THz metasensors primarily utilized aluminum (Al) due to its low cost and compatibility with flexible polymer substrates. Early designs demonstrated the potential for high sensitivity of 139.2 GHz/RIU, enabled by its topology for easy on-chip biosensing integration [32]. Subsequent Al-based work has focused on multi-band absorption and polarization-insensitive operation, achieving refractive index sensitivities in the range of 11–139.5 GHz/RIU [8, 21, 30, 32, 40-44]. A triple-band absorber on PET showed >86% absorption with sensitivities up to 139.5 GHz/RIU [40], while fractal geometries such as Pythagorean tree resonators were employed to enhance field localization, yielding sensitivities of 0.118 THz/RIU and suitability for biomedical hybrid sensing [8]. To improve plasmonic performance, researchers have shifted toward gold (Au)-based designs due to its high conductivity. These structures maintained high absorption (>99.5%) while offering geometrically tunable, dual-band operation with competitive refractive index sensitivities, exemplified by designs achieving up to 0.27 THz/RIU [9, 33]. On the other hand, copper-based metastructures are anticipated to offer a compelling alternative with enhanced functionality, owing to their higher electrical conductivity as well as advantageous balance of cost and availability compared to Au-based metastructures**. It is important to note that sensitivities exceeding 1 THz/RIU have been demonstrated in the literature [16, 18, 39, 45-50]. These high-sensitivity designs typically exploit Fano resonances [51] or quasi-BIC [52]. Moreover, such works generally employ all-dielectric [45, 46, 50] or hybrid [39, 49] resonators that operate at frequencies above 1.5 THz [16, 18, 39, 45-48, 50] or require expensive fabrication processes.**

This study introduces a THz metasurface, designed using a combination of copper circular rings and disk patterns with dual functions: an ideal **ultrathin** narrowband absorber and a **simulated high-sensitivity (under idealized conditions)** refractometer, suitable for detecting the refractive index of analytes. The proposed meta-structure is optimized to achieve perfect absorption at 0.8 THz, with resonant frequencies that can be flexibly tailored across 0.53 to 1.47 THz by modifying its geometric dimensions and dielectric permittivity. The design exhibits stable performance under a wide range of incident angles. To evaluate its sensing potential as a refractometer, we characterized the refractive index sensitivity by depositing a 25 μm analyte layer and then observing a significant resonance shift. Furthermore, the metasensor performance was evaluated under different substrate materials and through the replacement of copper with aluminum. This design offers a cost-effective and competitive solution, standing as an alternative to the more complex or less sensitive designs reported so far.

2. Structure design and simulation methods

The proposed THz metasurface absorber is illustrated schematically in Fig. 1. It features a periodic arrangement of circular-ring and disk-shaped copper resonators combined with a continuous metallic reflector layer, separated by a PTFE (Teflon) dielectric spacer (Cu|PTFE|Cu). This triple-layer structure efficiently confines incoming electromagnetic energy, resulting in significant field localization. Its simple design allows the metasurface to achieve near-perfect absorption performance.

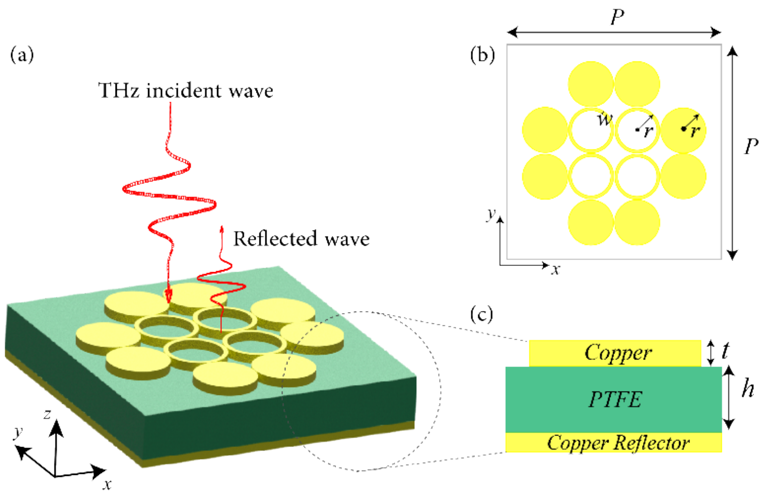

Fig. 1. Schematic structure of the proposed THz narrowband metasurface absorber (Cu|PTFE|Cu). (a) three-dimensional view of the meta-absorber, (b) top view, and (c) cross-section view of the unit cell.

The design parameters define the radii of the circular ring and disk as r=13 µm, with a ring width of w=1 µm. **The meta-structure unit cell period has a compact size of P=110 µm, $0.296\ \lambda_0 \times 0.296\ \lambda_0$, in which λ_0 denotes the wavelength corresponding to the resonance frequency.** Copper, with a conductivity of 5.8×10^7 S/m, is used for both the patterned resonators and the bottom reflector. The thicknesses of the top and bottom copper layers are t=1.9 µm and t_g=1 µm, respectively. The dielectric spacer consists of a h=4.1 µm-thick PTFE film, **equivalent to approximately $0.011\ \lambda_0$ (i.e., 1/91 of the resonance wavelength)**, with a relative permittivity $\varepsilon_r = 2.1$. **The use of this 4.1 µm dielectric substrate enables the resulting ultrathin architecture.**

Numerical simulations were performed using CST 2021 Microwave Studio to evaluate the absorption and sensing characteristics of the proposed THz metasurface. The S-parameters—reflection coefficient (S_{11}) and transmission coefficient (S_{21})—were computed applying unit cell boundary conditions along the x- and y-axes, and open boundary conditions along the z-axis. The metasurface was illuminated by a normally incident THz wave, and a frequency domain solver was employed to resolve the electromagnetic response. Due to the continuous metallic reflector, the **transmittance** ($T = |S_{21}|^2$) is effectively suppressed to zero, to ensure negligible wave propagation through the structure. Thus, the absorption A is derived from the reflection coefficient as $A = 1 - R$, where the **reflectance** $R = |S_{11}|^2$.

3. Results and discussions

3.1. Copper-based Metasurface performance as a narrowband perfect absorber

To optimize the performance of the proposed metasurface, a parametric study was performed by systematically varying three key geometric parameters: the unit cell period (*P*), the PTFE dielectric thickness (*h*), and the copper resonator thickness (*t*). In each case, one parameter was varied while the others were kept constant. The effect of the unit cell period is shown in Fig. 2(a). As *P* increases from 110 μm to 150 μm, the absorption peak undergoes a blue shift accompanied by a gradual decrease in intensity. **This behavior can be described using the equivalent LC resonant model [53]. According to this model, the capacitance between two neighboring unit cells decreases as the unit cell period, *P*, increases, leading to a shift of the absorption peak toward higher frequencies**. The maximum absorption intensity is achieved at the minimum period of *P*=110 μm. Figure 2(b) depicts the influence of the PTFE dielectric thickness, *h*, on the absorption spectrum. As *h* varies from 3.5 μm to 4.7 μm, the absorption is maximized at *h*=4.1 μm. A blue shift of the resonance **frequency** is also observed with increasing dielectric thickness. **This can also be explained, within the framework of the equivalent LC resonance model, by the reduction in capacitance between the resonators and the metallic reflector layer [53].** The impact of the copper resonator thickness, *t*, is illustrated in Fig. 2(c). The absorption spectrum was analyzed for *t* ranging from 0.7 μm to 2.7 μm, with peak absorption occurring at *t*=1.9 μm. Notably, variations in all three structural parameters of up to ±10% result in minimal shift of the resonant frequency. This insensitivity is advantageous, as it relaxes the fabrication tolerances required for device realization. The structural parameters of the copper-based THz metasurface optimized for maximum absorption are summarized in Table 1.

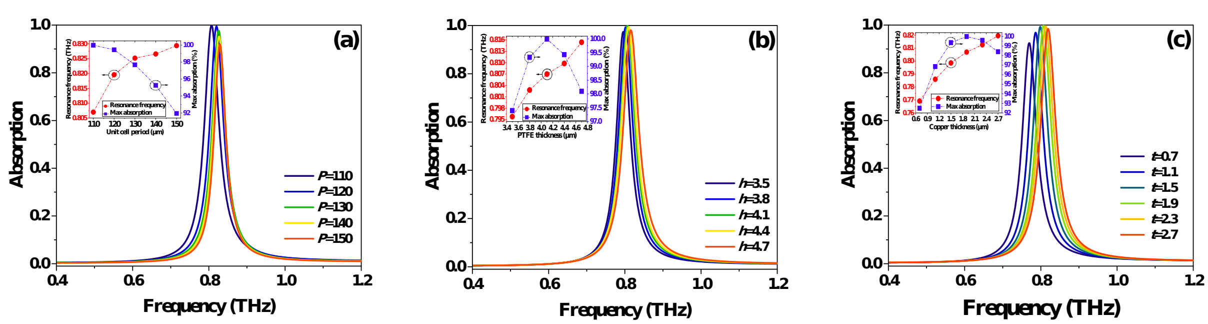

Fig. 2. Absorption of the proposed THz metasurface absorber versus the structural parameters, (a) unit cell period (*P*), (b) PTFE thickness (*h*), and (c) copper resonator thickness (*t*), under TE polarization.

Table 1. Optimized dimensions obtained for the proposed THz meta-absorber.

Parameter	Value (μm)	Description
t_g	1	Thickness of copper ground plane
t	1.9	Thickness of copper resonator

h	4.1	Thickness of PTFE dielectric substrate
P	110	Unit cell period
r	13	Disk and ring radius
w	1	Ring width

The optimal S-parameters and corresponding absorption spectra of the meta-absorber under normal incidence are presented in Fig. 3(a) for both transverse electric (TE) and transverse magnetic (TM) polarizations. The overlapped response of the S-parameters and absorption for the two polarization states clearly addresses the outstanding polarization insensitivity of the meta-absorber, which could be attributed to its symmetric geometry. Notably, perfect absorption (99.99%) is achieved at 0.807 THz (~ 0.8 THz) (FWHM=0.0566 THz, Q=14.26), accompanied by return losses of approximately 42.8 dB, which reflects the excellent performance characteristics. **This frequency lies within the 0.76–0.96 THz atmospheric transparency window, where low water vapor absorption enables practical operation in ambient air.** To elucidate the physical mechanism underlying perfect absorption, the distributions of electric and magnetic fields and surface current at the resonance frequency of 0.8 THz were simulated. Figures 3(b-d) present these distributions for both TE and TM polarizations. The electric field is strongly localized at the upper and lower edges of the horizontal disk patterns (Fig. 3(b)), exciting an electric dipole resonance aligned with the y-axis. Concurrently, the magnetic field is intensely concentrated in the gaps between adjacent resonators (Fig. 3(c)), signifying the formation of a magnetic dipole resonance. The observed field distributions are a direct consequence of the underlying current flow patterns, which can be either parallel or antiparallel. This is further corroborated by the surface current distribution (Fig. 3(d)), which forms closed loops around the ring resonators, a signature of magnetic dipole activity. Notably, the current density is maximum at the interfaces of the two diagonal disks, indicating regions of strong coupling with the incident THz waves. Furthermore, under TM polarization, the field distributions exhibit rotational symmetry while preserving their intensity profiles, indicating the polarization-insensitive behavior of the resonant frequency.

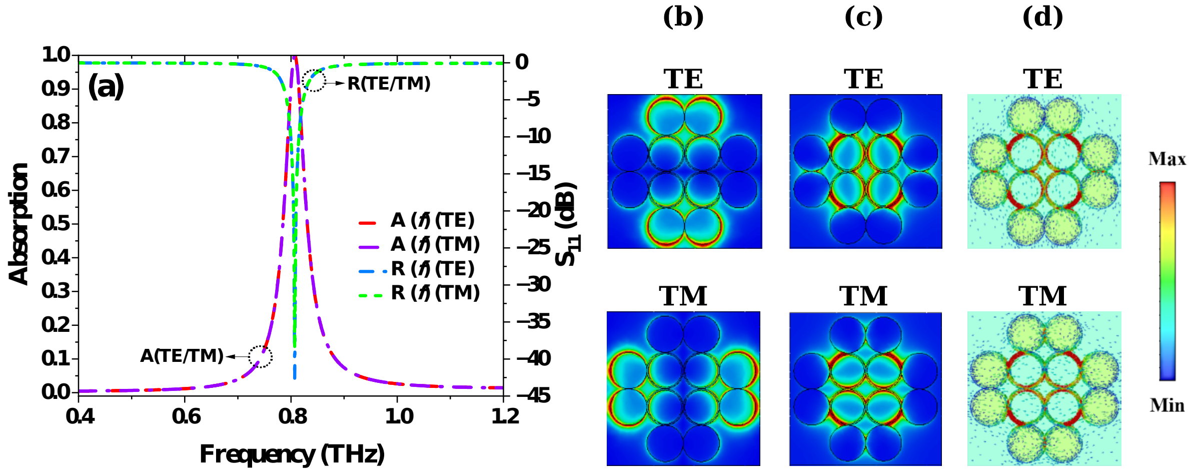

Fig. 3. (a) *S*-parameter (S_{11}) and absorption spectrum of the proposed metasurface absorber for TE and TM polarizations. (b) electric field, (c) magnetic field, and (d) top surface current distributions at the absorption peak of 0.8 THz for TE and TM polarizations.

The physical mechanism underlying the proposed THz meta-absorber is analyzed through impedance matching theory. For an MPA, optimal absorption occurs when the effective impedance of the metasurface, $Z(f)$, matches the impedance of free space (Z_0), thereby minimizing the reflection. The relative impedance is defined as

$$Z_r(f) = \frac{Z(f)}{Z_0} = \sqrt{\frac{(1 + S_{11}(f))^2 - S_{21}{}^2(f)}{(1 - S_{11}(f))^2 - S_{21}{}^2(f)}} \quad (1)$$

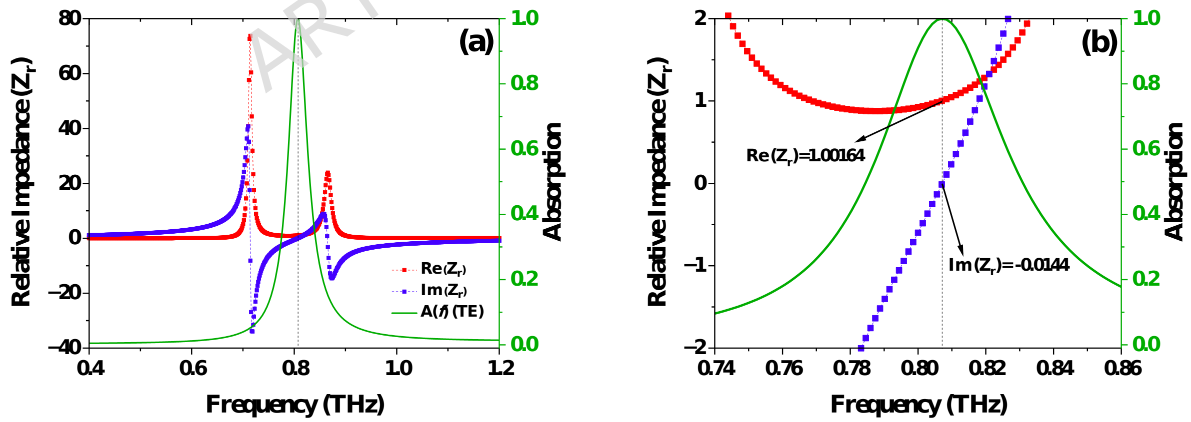

Fig. 4. Effective parameter analysis of the proposed THz-MPA. (a) Real and imaginary parts of relative impedance (which is magnified in (b)), under TE polarization.

As illustrated in Figs. 4(a,b), which presents the real and imaginary components of $Z_r(f)$ under normal incidence, this matching condition is achieved at the resonance frequency of 0.8 THz. At this point, the real part of $Z_r(f)$ is 1.00, and the imaginary part is approximately zero. This near-unity real part and negligible imaginary part confirm that the effective impedance of the meta-structure is closely matched to that of free space. Consequently, the incident THz wave is coupled efficiently into the meta-absorber, leading to the observed near-perfect absorption at the resonance frequency.

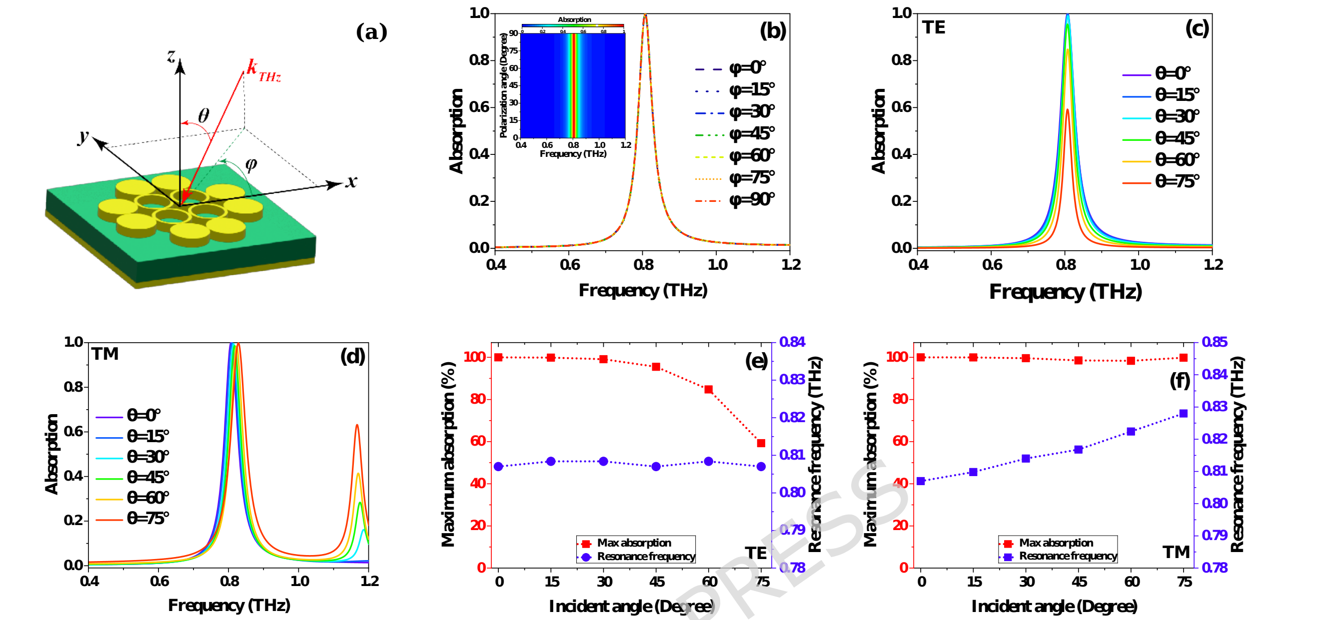

Fig. 5. (a) Schematic diagram of the polarization angle (φ) and the incidence angle (θ). Absorption of the proposed meta-absorber as a function of frequency at (b) various polarization angles from 0 to 90° (the inset shows the corresponding color map), and various incidence angles from 0 to 75° for both (c) TE and (d) TM polarizations. Maximum absorption at the resonance frequency and resonance frequency shift spectra as a function of the incidence angle for both (e) TE, and (f) TM polarizations.

Figure 5(a) illustrates the schematic of the proposed THz metasurface absorber, evaluated for various polarization states and under varying incidence angles. As depicted in Fig. 5(b), the absorber exhibits complete polarization insensitivity across the full range of polarization angles (φ = 0°–90°), which could be attributed to the symmetry of its circular-ring and disk geometry. Figures 5(c) and 5(d) present the absorption spectra for TE and TM polarizations, respectively, under incidence angles (θ) ranging from 0° to 75° (in 15° increments). Notably, the meta-absorber maintains high absorption (>90%) at the resonant frequency for θ = 45° and 75° in TE and TM polarizations, respectively. However, by increasing θ in the case of TM polarization, a secondary undesirable resonance appears at higher frequencies. In fact, an ideal metasurface absorber should exhibit stable absorption characteristics and minimal frequency shift across polarization and incidence angles. Figures 5(e) and 5(f) quantify the maximum absorption and resonant frequency shift as functions of θ for TE and TM polarizations. Minor deviations are observed at larger angles (θ = 45°–60°) in TE polarization, likely due to impedance mismatch. Overall, the absorber demonstrates robust performance, sustaining absorption levels above 80% across a wide angular range in TE polarization. Remarkably, at θ = 75° in TM polarization, peak absorption exceeds 99%. The resonant frequency shifts slightly with increasing θ, measured at 0.0014 THz for TE and 0.021 THz for TM at θ = 60° and θ = 75°, respectively. These shifts remain well below the spectral resolution of typical THz time-domain spectrometers (~0.03 THz or ~0.1 cm^{-1}) [54], underscoring the meta-absorber's angular resilience and spectral stability.

We further investigated the influence of structural parameters on the absorption characteristics of the proposed THz metasurface absorber. The effects of geometric variables *r* (radius of ring and disk) and *w* (ring width) were analyzed in Fig. 6(a) and 6(b), respectively. As *r* increases from 8 to 13.5 μm, the resonance absorption frequency exhibits a downward shift from 1.47 to 0.74 THz, corresponding to wavelengths of 204 and 405 μm**. Therefore, the resonance absorption frequency of the meta-absorber exhibits an approximately inverse relationship with the radius** r**, in agreement with the LC model based on equivalent circuit theory [55, 56], given by** $f = \frac{1}{2\pi\sqrt{LC}} \propto \frac{1}{r} \propto w$**, where *r* denotes the ring radius and *w* is the ring width. An increase in** r **leads to a higher equivalent inductance** L**, resulting in a progressive decrease of the resonance absorption frequency.** Conversely, increasing *w* from 0.5 to 10 μm results in an upward shift in resonance frequency from 0.78 to 0.94 THz, with associated wavelengths of 384 and 319 μm. **We have confirmed that this behavior can also be explained using the equivalent LC resonant circuit model.** Moreover, the resonance frequency can be **adjusted** via the relative permittivity ε_r of the dielectric substrate, as illustrated in Fig. 6(c). A decrease in resonance frequency is observed with increasing ε_r**. This behavior can also be explained using the equivalent LC resonant circuit model, given by** $f = \frac{1}{2\pi\sqrt{LC}} \propto \frac{1}{\sqrt{\varepsilon_r}}$ **[53]. An increase in the substrate's permittivity rises the capacitance between the resonator and the reflector layer, consequently shifting the resonance frequency to lower values.** Figures 6(d–f) collectively demonstrate the structural adjustability of the meta-absorber's resonance frequency across the 0.53–1.47 THz range by adjusting *r*, *w*, and ε_r. These results confirm that the meta-absorber's perfect absorption characteristics can be flexibly engineered through precise control of its geometrical and material parameters.

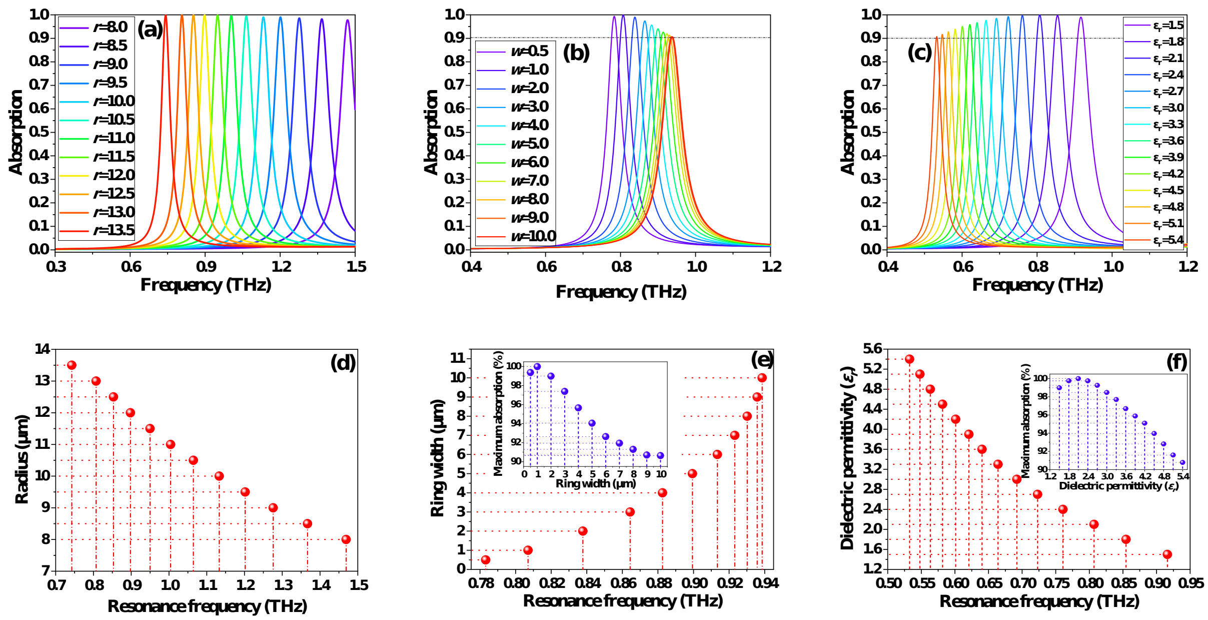

Fig. 6. Absorption of the proposed THz metasurface absorber versus the structure parameters (a) *r*, (b) *w*, and (c) ε_r, relative permittivity of the substrate. Dependence of (d) *r*, (e) *w*, and (f) ε_r on the resonance frequency.

A performance comparison between the proposed THz meta-absorber and several recently reported designs is summarized in Table 2. According to this comparison, it could be concluded that the proposed structure **shows competitive performance among the selected reported works under comparable simulation conditions —including similar resonator materials (metals), frequency bands, and incidence angles (normal incidence)**—in terms of absorption efficiency, wide-angle stability, adjustability, polarization independence, **ultra-thin thickness, compact unit cell**, and geometric simplicity. **These features could provide a robust platform for sensing, imaging, and material characterization. Furthermore, owing to its compact (0.296 λ_0) and ultrathin (0.011 λ_0) profile, the proposed design is well-suited for miniaturized integration.**

Table 2. Comparison of various narrowband THz meta-absorbers. **(λ_0 denotes the wavelength of the lowest resonance frequency)**

Resonator	**Frequency (THz)**	**No. of peaks**	**Absorption average**	**Angular stability**		**Polarization insensitivity**	**Adjustable structure**	**Difficulty of preparation**	λ_0 (μm)	**Dielectric thickness (μm)**	**Periodicity (μm)**	**Reference**
				TE	TM							
Al	0.59	1	99.9%	-	0-30°	Yes	Yes	Easy	508.12	0.016 λ_0	0.295 λ_0	2012 [57]
Au	1.71, 3.56	2	99.94%	0-40°	0-60°	Yes	No	Rather easy	175.317	2.85 λ_0	0.285 λ_0	2011 [58]
	1.80, 2.97	2	98%	-	-	No	Yes	Rather easy	166.55	0.022 λ_0	0.36 λ_0	2016 [59]
	1.15	1	99.13%	0-40°	0-80°	Yes	No	Difficult	260.689	0.025 λ_0	0.307 λ_0	2017 [60]

	0.61, 1.68	2	99.1%	-	-	No	Yes	Rather easy	491.46	0.0305 λ_0	0.244 λ_0	2022 [61]
	0.72, 1.01	2	95%	0-30°	0-30°	Yes	No	Rather difficult	416.378	0.6 λ_0	0.08 λ_0	2023 [62]
	0.6, 1.2	2	-	0-50°	0-50°	Yes	Yes	Rather easy	499.654	0.02 λ_0	0.28 λ_0	2023 [9]
Cu	0.807	1	99.99%	0-45°	0-75°	Yes	Yes	Easy	371.49	0.011 λ_0	0.296 λ_0	Present work

3.2. Copper-based Metasurface performance as an analyte sensor

To assess the biosensing capabilities of the proposed THz meta-absorber, its absorption spectrum in the vicinity of an analyte was numerically simulated. The analyte was regarded as a layer deposited on the top surface of the meta-absorber, as illustrated in Fig. 7. The metasensor's performance was evaluated through a two-stage computational analysis. In the first stage, the sensitivity was examined for various analyte thicknesses, while its refractive index was kept fixed at $n = 1.73$, corresponding to typical biological media [32]. In the second stage, refractive index sensitivity was analyzed by sweeping n from 1.0 to 2.0 under a constant analyte thickness. The performance of the metasensor is quantitatively characterized by three key metrics: sensitivity (S), figure of merit (FoM), and quality factor (Q-factor). The S defines the metasensor's responsivity to changes in the local dielectric environment, which is calculated as the shift in resonant frequency per unit change in the refractive index, as $S = \Delta f/\Delta n$. Here Δf denotes the resonance frequency shift, and Δn is the change in the refractive index of the analyte, measured in refractive index units (RIU). The FoM provides a more comprehensive performance criterion by normalizing the sensitivity to the resonance linewidth, thus accounting for the sharpness of the resonance as $FoM = S/FWHM$. Finally, the Q-factor is a direct measure of the resonance sharpness, defined as $Q = f_r/FWHM$, where f_r is the central resonant frequency. **This study presents numerical simulations conducted under idealized lossless and noise-free conditions, with perfectly defined layer interfaces. Therefore, the practical features of the sensor would be affected in realistic biological conditions, which are typically lossy, water-containing, and heterogeneous.**

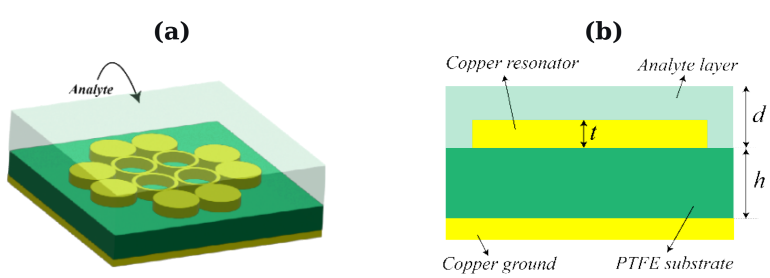

Fig. 7. Schematic diagram of the proposed THz meta-absorber for analyte sensing. (a) Copper-based THz meta-absorber structure covered by an analyte layer (blue part), and (b) the cross-sectional view of the metasensor.

3.2.1. Analyte's thickness sensor

Detailed simulations were conducted to quantify the sensitivity of the metasensor's resonance frequency to variations in analyte thickness (*d*). The meta-absorber was coated with a dielectric overlayer ($\varepsilon = 3$, $n \approx 1.73$) with a thickness that was varied from 1 to 50 µm. As shown in Fig. 8(a), increasing the analyte thickness induces a redshift in the resonant frequency, as presented in Fig. 8(b). The resonant frequency saturates at an analyte thickness of approximately 30 µm (orange part in Fig. 8(b)), indicating that the electromagnetic field interaction is confined to a finite penetration depth. The shift in resonant frequency ($\Delta f = f_d - f_{d=0}$) as a function of analyte thickness follows a bi-exponential saturation trend, fitted by $\Delta f = 0.131 - [(0.05 \times e^{-d/2.37}) + (0.079 \times e^{-d/8.45})]$ (THz). When the analyte thickness is below 25 µm, the resonance frequency exhibits a rapid shift with increasing thickness. Beyond this threshold, the metasensor demonstrates a pronounced saturation effect, indicating diminished sensitivity gains. **Therefore, if this sensor were used in a practical application, operating with an analyte thickness below 25 µm would yield higher sensitivity, as the frequency shift per unit thickness is largest in this regime.** It is important to note that the saturation threshold is influenced by both the structural design and the material composition of the metasurface [14]. **To evaluate the metasensor's sensitivity in the ultrathin regime (below 5 µm), the relationship between resonant frequency shift and analyte layer thickness was analyzed (green part in Fig. 8(b)).** A linear fit to the data yields the function $\Delta f = f_d - f_{d=1} = [(0.01403 \times d) - 0.0118]$ (THz), with a high coefficient of determination ($R^2 = 0.988$) (Fig. 8c). This corresponds to a thickness sensitivity (the slope of the linear fitting function) of 14 GHz/µm, much larger than those previously reported in the THz regime [28, 29, 63, 64].

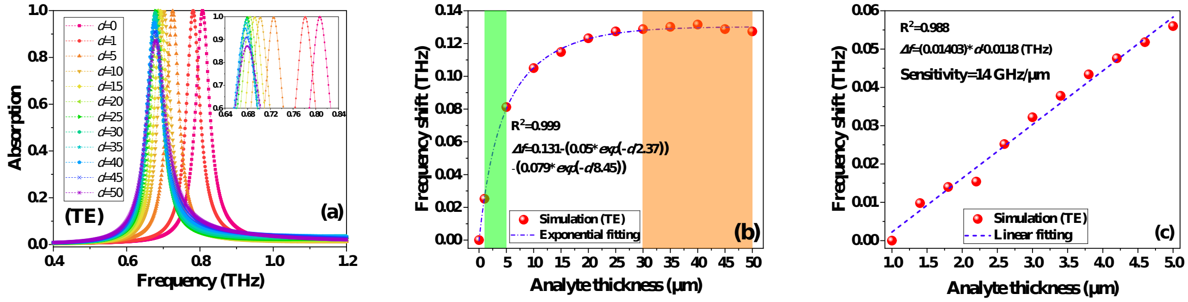

Fig. 8. (a) Absorption spectrum of the metasensor for different *d*, thicknesses of the analyte layer. (b) Relative change in resonance frequency of the metasensor with changing analyte layer thickness. The blue dashed line shows the exponential fitting of the simulation results. (c) Resonance frequency shift for ultrathin analyte layer thickness (1–5 μm); the blue dashed lines are the linear fitting results of the simulated data.

3.2.2. Analyte's refractive index sensor

To quantify the refractive index sensitivity of our design, a lossless analyte layer with a refractive index varying from 1.0 to 2.0 was modeled. An analyte layer thickness of 25 μm was selected to provide a near-perfect absorption efficiency (> 99%) and ensure a strong resonant signal across the entire index range. Figure 9(a) presents the simulation results, revealing a significant redshift in the resonant frequency as the analyte's refractive index increases from 1.0 to 2.0 in 0.1 increments under normal incidence. The frequency shift, which directly reflects the sensitivity of the metasensor, is plotted as a function of the analyte's refractive index in Fig. 9(b). A linear increase in resonance frequency shift is observed, indicating a proportional sensing response. To quantify this behavior, linear fitting was applied to the data, yielding the expression $\Delta f = 0.173 \times n - 0.172$ (THz) with an R^2 value of 0.999. The maximum frequency shift reaches approximately 173 GHz for the resonant mode, corresponding to a frequency sensitivity ($S = \frac{d\Delta f}{dn}$) of 173 GHz per RIU. Figure 9(c) plots the FWHM and the Q-factor of the proposed metasensor as a function of the analyte refractive index. A maximum Q-factor of 14.29 is achieved for a refractive index of 1.0 (air), confirming a strong electromagnetic interaction within the meta-structure. The Q-factor then slightly decreases with increasing refractive index, reaching a minimum of 12.76 for TE polarization at n = 2.0. This trend indicates that radiative losses are lowest in air and highest at n=2.0. Furthermore, at n=2.0, the metasensor achieves a FoM of approximately 3.47, a value that **is** significantly **competitive among selected previous works** [23, 30] and underscores its effective performance even for high-index analytes. Figure 9(d) depicts the frequency sensitivity as a function of the incident angle for both TE and TM polarizations. The results indicate that the sensitivity remains largely stable across the angular range from 0° to 75°, with the TE polarization exhibiting superior angular stability. At normal incidence (0°), the sensitivity is higher for TE polarization (0.173 THz/RIU) than for TM polarization (0.169 THz/RIU). The frequency shift resulting from variations in analyte thickness (Fig. 8b) was used to evaluate the dependence of the sensor's frequency sensitivity on analyte thickness, as shown in Fig. 9(e). The frequency sensitivity values exhibit exponential growth, described by the fitting function $S = 0.183 - [(0.062 \times e^{-d/1.51}) + (0.12 \times e^{-d/7.92})]$ with an R^2 value of 0.998, where d is the analyte thickness. Increases the thickness, the refractive index sensitivity improves, reaching a maximum value of approximately 0.177 THz/RIU for thicknesses beyond 40 μm. However, this enhancement is accompanied by a reduction in absorption amplitude, reflected in an increasing amplitude difference. As illustrated in Fig. 9(f), the absorption amplitude remains nearly constant up to 25 μm, which is a desirable characteristic for sensing applications. However, between 25 and 50 μm, the amplitude difference increases linearly, providing a potential basis for designing sensors that exploit changes in absorption amplitude.

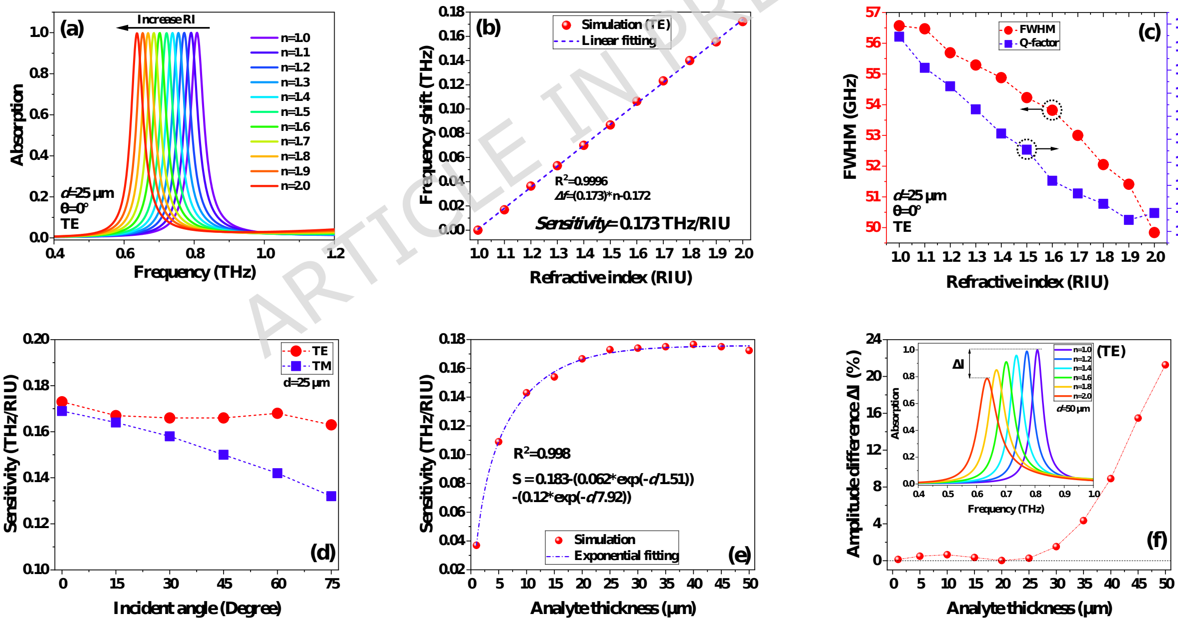

Fig. 9. Sensing performance of the proposed copper-based meta-absorber (Cu|PTFE|Cu|analyte). (a) Absorption spectra for various refractive indices from 1.0 to 2.0, and (b) frequency shift (Δf) versus analyte refractive index for the resonant mode for TE polarization. (c) FWHM and quality factor of the proposed metasensor at different refractive indexes. (d) Frequency sensitivity as a function of incident angle, ranging from 0° to 75°, for TE and TM polarizations. (e) Frequency sensitivity and (f) amplitude difference of the resonant mode as a function of the analyte thickness (the inset shows the absorption spectra for analytes of different refractive indices at a fixed thickness (d = 50 μm)).

The sensing performance was further examined using two commercially available and widely reported substrate materials: TOPAS ($\varepsilon = 2.35$) and polyimide (PI, $\varepsilon = 3.5$). For each substrate, the analyte's refractive index was varied from 1.0 to 2.0 in increments of 0.2 under TE polarization. For the metasensor based on TOPAS substrate (Cu|TOPAS|Cu|analyte), Fig. 10(a) shows a significant redshift in resonant frequency with increasing refractive index. The resulting frequency shift, plotted in Fig. 10 (b), yields a sensitivity of 149 GHz/RIU. As shown in Fig. 10(c), the Q-factor decreases slightly as the refractive index increases, reaching a minimum of 13.02. At this point, the metasensor achieves a FoM of approximately 3.13. Similarly, for the metasensor based on PI substrate (Cu|PI|Cu|analyte), a pronounced redshift is observed in Fig. 11(a). The frequency sensitivity derived from Fig. 11(b) is 93.8 GHz/RIU. Figure 11(c) illustrates the corresponding FWHM and Q-factor trends, with the Q-factor declining to a minimum of 13.55. The resulting FoM at n= 2.0 is approximately 2.31. Overall, these results confirm that the proposed copper-based metasurface employing a Teflon substrate exhibits superior sensitivity and FoM compared to that with TOPAS and PI substrates, thereby offering enhanced performance for biosensing applications.

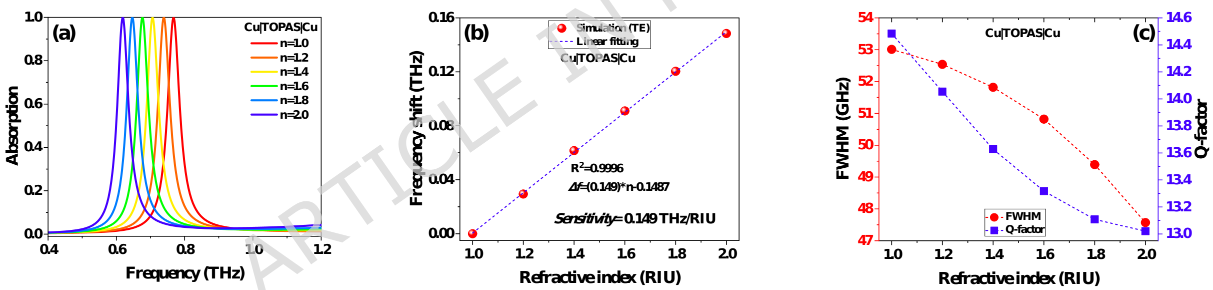

Fig. 10. Sensing performance of the proposed Copper-based meta-absorber with TOPAS substrate (Cu|TOPAS|Cu|analyte). (a) Absorption spectra with changing refractive index ranging from 1.0 to 2.0 (fixed analyte thickness d=25 μm), and (b) Frequency shift (Δf) versus analyte refractive index for the resonant mode for TE polarization. (c) FWHM and quality factor of the Cu|TOPAS|Cu metasensor at different refractive indexes.

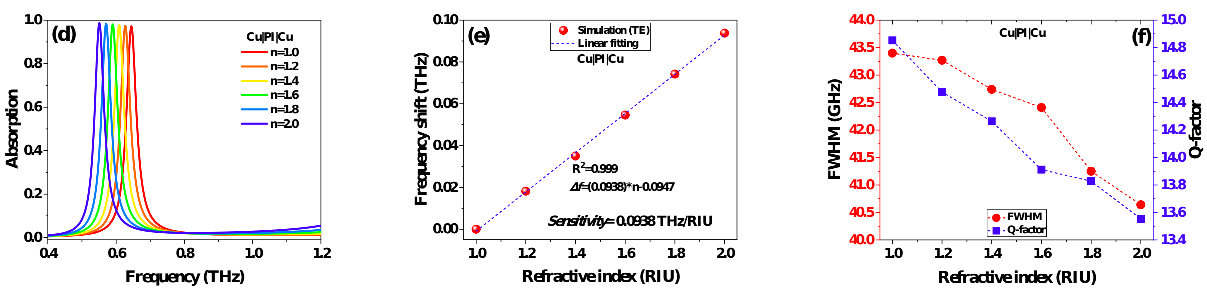

Fig. 11. Sensing performance of the proposed Copper-based meta-absorber with polyimide substrate (Cu|PI|Cu|analyte). (a) Absorption spectra with changing refractive index ranging from 1.0 to 2.0 (fixed analyte thickness d=25 μm), and (b) Frequency shift (Δf) versus analyte refractive index for the resonant mode for TE polarization. (c) FWHM and quality factor of the Cu|PI|Cu metasensor at different refractive indexes.

3.3. Alternative candidate for copper-based metasensor

We have further examined the performance of the proposed meta-structure when its metallic components were substituted with aluminum, which could be motivated by its lower cost and accessibility. To achieve optimal absorption, the dimensions of the aluminum-based design were kept identical to those listed in Table 1, except the PTFE substrate thickness (4.2 µm) and the Al resonator thickness (2.5 µm). Figure 12(a) presents the absorption spectrum of the aluminum-based meta-absorber alongside that of its copper-based counterpart. The Al-based structure resonates at 0.814 THz with a FWHM of 0.0659 THz, yielding a $Q = 12.35$. The broader linewidth—and correspondingly lower Q—relative to the copper-based meta-absorber is attributed to the higher ohmic losses inherent to aluminum. Figure 12(b) illustrates the resonance shift of the aluminum-based metasensor when covered with a 25 µm analyte layer (Al|PTFE|Al|analyte). The derived sensitivity is 0.178 THz/RIU, nearly identical to that of the copper-based metasensor. However, as shown in Fig. 12(c), both the Q factor and FWHM degrade with increasing analyte refractive index, with Q dropping to 11.34. The resulting FOM for the Al-based metasensor is 3.16. In summary, while aluminum offers a viable alternative to copper in terms of sensitivity and significant cost advantages, this substitution comes at the expense of reduced Q factor and overall FOM, primarily due to the higher losses of aluminum. A comparative summary with those in recent literature, shown in Table 3, emphasizes the strong performance of the proposed copper-based THz metasensor. Utilizing PTFE and TOPAS dielectrics, it delivers a noteworthy combination of high sensitivity and FoM.

To ensure fair comparison, prior works were selected based on similarity to our simulation conditions: (i) same resonator material (e.g., metals), (ii) comparable frequency band (≤ 1.5 THz), and (iii) similar incidence angle (normal). Nevertheless, residual inconsistencies remain across studies (e.g., analyte thickness). Therefore, our claim is not superior but rather competitive performance within the selected set under idealized conditions.

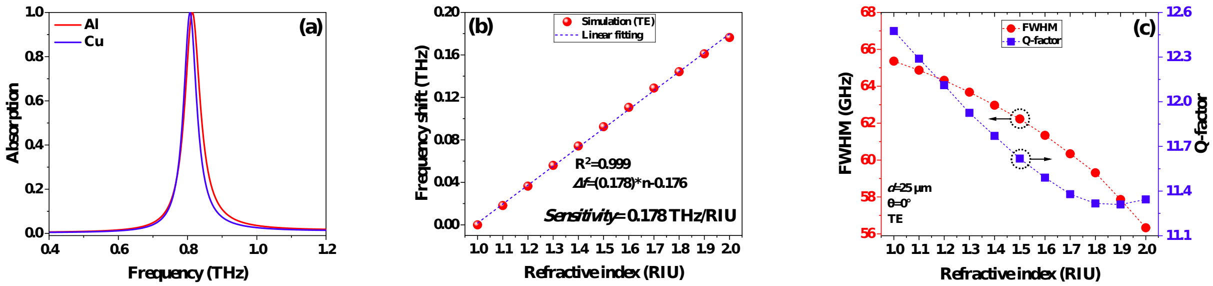

Fig. 12. (a) Comparing the absorption spectra of Cu-based (Cu|PTFE|Cu) and Al-based (Al|PTFE|Al) meta-absorbers. **(b)** Frequency shift (Δf) versus analyte refractive index, (c) FWHM and quality factor of the metasensor based on Al (fixed analyte thickness d=25 μm) at different refractive indexes under TE polarization.

Table 3. Comparative performance metrics of prior refractive index metasensors **(with similar metal resonator, frequency band, and incidence angle)** and the proposed metasurface design.

Resonator	Meta-atom configuration	Substrate material	Resonance frequency (THz)	RI Sensitivity (THz/RIU)	FoM	Reference
Al	Two-gap split ring	Kapton polyimide	0.76	0.1392	-	2015 [32]
	Outer square SRR & inner circular SRR & two short bars	Si	0.85	0.085	-	2019 [41]
	H-shape & U-shape	Si	0.96	0.085	-	2020 [42]
	Ring with a cross notch	quartz	0.835	0. 135	-	2021 [21]
	Three concentric square rings	PET	0.718	0.1395	-	2021 [40]
	Pythagorean tree fractal	PET	0.69	0.1182	-	2022 [8]
	Asymmetric split rings	SiO_2	0.801	0.124	-	2022 [43]
	Two isosceles triangles & a rectangular connecting block	Si	0.89	0.011	-	2022 [44]
	Multi ring	PET	0.797	0.076	1.15	2023 [30]
Au	Split ring	Si	0.5	0.055	0.43	2017 [23]
			1.16	0.118	0.17	
	Three-split ring	Si	0.68	0.0489	0.543	2022 [65]
			1.627	0.0732	0.191	
	Two split-ring	SiO_2	0.828	0. 103	-	2023 [15]
	Circular-ring & cross-shape	benzocyclobutene (BCB)	0.6	0.13	5	2023 [9]
	Square ring with T-shaped strips	Si	1.36	0.037	3.3	2023 [33]
Cu	Split I-shape	quartz	0.88	0.1246	-	2023 [26]
Cu	Disk & ring	PTFE	0.807	TE: 0.173	3.47	Present work
				TM: 0.169	3.38	
		TOPAS	0.768	TE: 0.149	3.13	
Al		PTFE	0.814	TE: 0.178	3.16	

4. Conclusion

We have numerically demonstrated a dual-function THz metasurface based on copper ring–disk resonators, serving as both a narrowband ultrathin absorber and a refractive-index/thickness sensor. The meta-structure achieves near-perfect absorption at 0.8 THz with

polarization insensitivity and wide-angle stability (up to 45° for TE, 75° for TM). Simulated sensitivity reaches 0.173 THz/RIU for refractive index and 14 GHz/μm for thickness variations—competitive with selected prior numerical studies. PTFE outperforms TOPAS and PI as a substrate, while aluminum offers comparable sensitivity but reduced Q-factor and FoM. This copper-based metasurface provides a simple, cost-effective, and numerically promising platform for THz sensing applications.

Data availability

Data underlying the results presented in this paper are not publicly available at this time but may be obtained from the authors upon reasonable request.

References

[1] D. Wu *et al.*, "Ultra-narrow band perfect absorber and its application as plasmonic sensor in the visible region," *Nanoscale research letters,* vol. 12, no. 1, p. 427, 2017.
[2] W. Ali, W. Liu, Y. Liu, and Z. Li, "Near-infrared perfect absorption and refractive index sensing enabled by split ring nanostructures," *Nanomaterials,* vol. 13, no. 19, p. 2668, 2023.
[3] S. M. Hosseini, F. Jahangiri, and H. Latifi, "Bandwidth improvement in copper-based terahertz metamaterial absorbers by structural engineering," *Optics Express,* vol. 33, no. 17, pp. 35336-35351, 2025.
[4] S. M. Hosseini and F. Jahangiri, "A Spacer-Thickness Tunable Terahertz Metasurface Absorber for Wide-Angle and Polarization-Insensitive Operation," *Pioneering Advances in Materials,* vol. 1, no. 2, pp. 37-45, 2026.
[5] T. Amini, F. Jahangiri, Z. Ameri, and M. A. Hemmatian, "A review of feasible applications of THz waves in medical diagnostics and treatments," *Journal of Lasers in Medical Sciences,* vol. 12, p. e92, 2021.
[6] B. M. Fischer, M. Walther, and P. U. Jepsen, "Far-infrared vibrational modes of DNA components studied by terahertz time-domain spectroscopy," *Physics in Medicine & Biology,* vol. 47, no. 21, p. 3807, 2002.
[7] B. M. Fischer *et al.*, "Terahertz time-domain spectroscopy and imaging of artificial RNA," *Optics Express,* vol. 13, no. 14, pp. 5205-5215, 2005.
[8] Y. I. Abdulkarim *et al.*, "Highly sensitive dual-band terahertz metamaterial absorber for biomedical applications: simulation and experiment," *ACS omega,* vol. 7, no. 42, pp. 38094-38104, 2022.
[9] H. Zhu *et al.*, "Dual-band terahertz metamaterial absorber and its refractive-index-sensing application for material films," *ACS Applied Optical Materials,* vol. 1, no. 7, pp. 1281-1288, 2023.
[10] H. Sahoo, "Fluorescent labeling techniques in biomolecules: a flashback," *RSC advances,* vol. 2, no. 18, pp. 7017-7029, 2012.
[11] R. J. Beynon and J. M. Pratt, "Metabolic labeling of proteins for proteomics," *Molecular & Cellular Proteomics,* vol. 4, no. 7, pp. 857-872, 2005.
[12] M. Gupta and R. Singh, "Terahertz sensing with optimized Q/Veff metasurface cavities," *Advanced Optical Materials,* vol. 8, no. 16, p. 1902025, 2020.
[13] R. Singh, W. Cao, I. Al-Naib, L. Cong, W. Withayachumnankul, and W. Zhang, "Ultrasensitive terahertz sensing with high-Q Fano resonances in metasurfaces," *Applied Physics Letters,* vol. 105, no. 17, 2014.

[14] L. Cong, S. Tan, R. Yahiaoui, F. Yan, W. Zhang, and R. Singh, "Experimental demonstration of ultrasensitive sensing with terahertz metamaterial absorbers: A comparison with the metasurfaces," *Applied Physics Letters,* vol. 106, no. 3, 2015.

[15] W. Liu *et al.*, "High sensitive and specific detection of SCCA via halloysite nanotube modified terahertz metasurface sensor," *IEEE Sensors Journal,* vol. 23, no. 7, pp. 6728-6733, 2023.

[16] R. Bhati and A. K. Malik, "Ultra-efficient terahertz metamaterial sensor," *Results in Optics,* vol. 8, p. 100236, 2022.

[17] X. Deng *et al.*, "Terahertz metamaterial sensor for sensitive detection of citrate salt solutions," *Biosensors,* vol. 12, no. 6, p. 408, 2022.

[18] X. Chen and W. Fan, "Ultrasensitive terahertz metamaterial sensor based on spoof surface plasmon," *Scientific reports,* vol. 7, no. 1, p. 2092, 2017.

[19] W. Cai, J. Zhu, Y. Yang, X. Wang, Z. Qian, and S. Fan, "High performance of terahertz sensor based on double-split hexagonal ring metamaterial," *IEEE Sensors Journal,* vol. 23, no. 19, pp. 22414-22420, 2023.

[20] X. Du *et al.*, "Highly sensitive detection of plant growth regulators by using terahertz time-domain spectroscopy combined with metamaterials," *Optics Express,* vol. 29, no. 22, pp. 36535-36545, 2021.

[21] X. Hou, X. Chen, T. Li, Y. Li, Z. Tian, and M. Wang, "Highly sensitive terahertz metamaterial biosensor for bovine serum albumin (BSA) detection," *Optical Materials Express,* vol. 11, no. 7, pp. 2268-2277, 2021.

[22] L. Cao *et al.*, "Terahertz metamaterial sensors: design theory, optimization approach, and advancements in biosensing applications," *Advanced Materials Technologies,* vol. 10, no. 9, p. 2401358, 2025.

[23] M. Islam, S. J. M. Rao, G. Kumar, B. P. Pal, and D. Roy Chowdhury, "Role of resonance modes on terahertz metamaterials based thin film sensors," *Scientific reports,* vol. 7, no. 1, p. 7355, 2017.

[24] R. Bhati, M. Jewariya, and A. K. Malik, "Spoof surface plasmon-based terahertz metasensor for glucose and ethanol," *Applied Physics A,* vol. 128, no. 9, p. 840, 2022.

[25] M. N. Hamza *et al.*, "Terahertz dual-band metamaterial biosensor for cervical-cancer diagnostics," *IEEE Photonics Journal,* 2024.

[26] X. Zhang, X. Wu, B. Xiao, and J. Qin, "Terahertz determination of imidacloprid in soil based on a metasurface sensor," *Optics Express,* vol. 31, no. 23, pp. 37778-37788, 2023.

[27] N. Cui *et al.*, "High electric field-enhanced terahertz metamaterials with bowtie triangle rings: modeling, mechanism, and carbohydrate antigen 125 detection," *The Journal of Physical Chemistry C,* vol. 125, no. 35, pp. 19374-19381, 2021.

[28] X. Zhou *et al.*, "Design, simulation, and experimental realization of a high-sensitivity polarization-independent electromagnetically induced transparent terahertz metamaterials," *Optics express,* vol. 32, no. 19, pp. 33130-33143, 2024.

[29] X. Zhang *et al.*, "Carbon nanotube-based flexible metamaterials for THz sensing," *Optical Materials Express,* vol. 11, no. 5, pp. 1470-1483, 2021.

[30] M. N. Hamza and M. T. Islam, "Designing an extremely tiny dual-band biosensor based on MTMs in the terahertz region as a perfect absorber for non-melanoma skin cancer diagnostics," *IEEE Access,* vol. 11, pp. 136770-136781, 2023.

[31] H. Bahador, "Five-segment THz refractive index metamaterial biosensor with perfect absorption for carcinoembryonic antigen measurement," *IEEE Sensors Journal,* 2024.
[32] R. Yahiaoui, S. Tan, L. Cong, R. Singh, F. Yan, and W. Zhang, "Multispectral terahertz sensing with highly flexible ultrathin metamaterial absorber," *Journal of Applied Physics,* vol. 118, no. 8, 2015.
[33] D. Wang, K.-D. Xu, S. Luo, Y. Cui, L. Zhang, and J. Cui, "A high Q-factor dual-band terahertz metamaterial absorber and its sensing characteristics," *Nanoscale,* vol. 15, no. 7, pp. 3398-3407, 2023.
[34] R. K. Singh, P. Binda, and U. Dey, "Investigations on a Triple-Band Metasurface Absorber as THz-Biomedical Sensor," *IEEE Transactions on Plasma Science,* 2024.
[35] X. Yan, L.-J. Liang, X. Ding, and J.-Q. Yao, "Solid analyte and aqueous solutions sensing based on a flexible terahertz dual-band metamaterial absorber," *Optical Engineering,* vol. 56, no. 2, pp. 027104-027104, 2017.
[36] F. Ahmed, M. A. Azim, and A. Zubair, "High sensitivity terahertz metamaterial sensor for trace pesticide detection," *RSC advances,* vol. 15, no. 26, pp. 20530-20541, 2025.
[37] L. Ma, Y. Liu, Y. Zhu, and W. Gu, "Sensing performance of triple-band terahertz metamaterial absorber based on snowflake-shaped resonators," in *Photonics*, 2022, vol. 9, no. 10: MDPI, p. 777.
[38] A. S. Saadeldin, M. F. O. Hameed, E. M. Elkaramany, and S. S. Obayya, "Highly sensitive terahertz metamaterial sensor," *IEEE Sensors Journal,* vol. 19, no. 18, pp. 7993-7999, 2019.
[39] M. Karthikeyan, P. Jayabala, S. Ramachandran, S. S. Dhanabalan, T. Sivanesan, and M. Ponnusamy, "Tunable optimal dual band metamaterial absorber for high sensitivity THz refractive index sensing," *Nanomaterials,* vol. 12, no. 15, p. 2693, 2022.
[40] J. Wang, T. Lang, Z. Hong, M. Xiao, and J. Yu, "Design and fabrication of a triple-band terahertz metamaterial absorber," *Nanomaterials,* vol. 11, no. 5, p. 1110, 2021.
[41] Y. Li *et al.*, "Four resonators based high sensitive terahertz metamaterial biosensor used for measuring concentration of protein," *Journal of Physics D: Applied Physics,* vol. 52, no. 9, p. 095105, 2019.
[42] D. Li, S. Lin, F. Hu, Z. Chen, W. Zhang, and J. Han, "Metamaterial terahertz sensor for measuring thermal-induced denaturation temperature of insulin," *IEEE Sensors Journal,* vol. 20, no. 4, pp. 1821-1828, 2019.
[43] D. Li *et al.*, "Terahertz metamaterial biosensor for diagnosis of hepatocellular carcinoma at early stage," *Applied Optics,* vol. 61, no. 16, pp. 4817-4822, 2022.
[44] X. Liu *et al.*, "Terahertz metasurfaces based on bound states in the continuum (BIC) for high-sensitivity refractive index sensing," *Optik,* vol. 261, p. 169248, 2022.
[45] Z. Wu, J. Tian, and R. Yang, "A graphene based dual-band metamaterial absorber for TE polarized THz wave," *Micro and Nanostructures,* vol. 168, p. 207331, 2022.
[46] G. Varshney and P. Giri, "Bipolar charge trapping for absorption enhancement in a graphene-based ultrathin dual-band terahertz biosensor," *Nanoscale Advances,* vol. 3, no. 20, pp. 5813-5822, 2021.

ARTICLE IN PRESS

[47] H. Bahador, "Five-segment THz refractive index metamaterial biosensor with perfect absorption for carcinoembryonic antigen measurement," *IEEE Sensors Journal,* vol. 24, no. 16, pp. 25715-25723, 2024.
[48] A. G. Mazare *et al.*, "Enhanced sensing capacity of terahertz triple-band metamaterials absorber based on Pythagorean fractal geometry," *Materials,* vol. 15, no. 18, p. 6364, 2022.
[49] C. Li and Q. Wu, "Graphene-based tunable high-sensitivity metasurface refractive index sensor," *Plasmonics,* vol. 20, no. 2, pp. 951-962, 2025.
[50] S. Ma, P. Zhang, X. Mi, and H. Zhao, "Highly sensitive terahertz sensor based on graphene metamaterial absorber," *Optics Communications,* vol. 528, p. 129021, 2023.
[51] S. Karmakar, D. Kumar, R. K. Varshney, and D. R. Chowdhury, "Strong terahertz matter interaction induced ultrasensitive sensing in Fano cavity based stacked metamaterials," *Journal of Physics D: Applied Physics,* vol. 53, no. 41, p. 415101, 2020.
[52] L. Zhang, H. Shen, and Z. Huang, "Polarization-independent dual-band quasi-bound states in the continuum based on graphene metasurface for tunable THz sensing application," *Scientific Reports,* vol. 15, no. 1, p. 11887, 2025.
[53] X. Ling, Z. Xiao, and X. Zheng, "Tunable terahertz metamaterial absorber and the sensing application," *Journal of Materials Science: Materials in Electronics,* vol. 29, no. 2, pp. 1497-1503, 2018.
[54] P. Han, M. Tani, M. Usami, S. Kono, R. Kersting, and X.-C. Zhang, "A direct comparison between terahertz time-domain spectroscopy and far-infrared Fourier transform spectroscopy," *Journal of Applied Physics,* vol. 89, no. 4, pp. 2357-2359, 2001.
[55] F. Chen, Y. Cheng, and H. Luo, "Temperature tunable narrow-band terahertz metasurface absorber based on InSb micro-cylinder arrays for enhanced sensing application," *IEEE Access,* vol. 8, pp. 82981-82988, 2020.
[56] Z. Li, T. Wang, L. Qu, H. Zhang, D. Li, and Y. Zhang, "Design of bi-tunable triple-band metamaterial absorber based on Dirac semimetal and vanadium dioxide," *Optical Materials Express,* vol. 10, no. 8, pp. 1941-1950, 2020.
[57] H. Kong, G. Li, Z. Jin, G. Ma, Z. Zhang, and C. Zhang, "Polarization-independent metamaterial absorber for terahertz frequency," *Journal of Infrared, Millimeter, and Terahertz Waves,* vol. 33, no. 6, pp. 649-656, 2012.
[58] X.-J. He, Y. Wang, J. Wang, T. Gui, and Q. Wu, "Dual-band terahertz metamaterial absorber with polarization insensitivity and wide incident angle," *Progress In Electromagnetics Research,* vol. 115, pp. 381-397, 2011.
[59] B.-X. Wang, G.-Z. Wang, and L.-L. Wang, "Design of a novel dual-band terahertz metamaterial absorber," *Plasmonics,* vol. 11, no. 2, pp. 523-530, 2016.
[60] M. D. Astorino, F. Frezza, and N. Tedeschi, "Ultra-thin narrow-band, complementary narrow-band, and dual-band metamaterial absorbers for applications in the THz regime," *Journal of Applied Physics,* vol. 121, no. 6, 2017.
[61] B.-X. Wang, W. Xu, Y. Wu, Z. Yang, S. Lai, and L. Lu, "Realization of a multi-band terahertz metamaterial absorber using two identical split rings having opposite opening directions connected by a rectangular patch," *Nanoscale Advances,* vol. 4, no. 5, pp. 1359-1367, 2022.
[62] D. Wang *et al.*, "Dual-band terahertz absorber based on square ring metamaterial structure," *Optics Express,* vol. 31, no. 4, pp. 5940-5950, 2023.

[63] H. Zhang, C. Liu, C. Xu, Z. Li, Y. Wang, and Y. Peng, "A dual-band terahertz metamaterial sensor with high Q-factor and sensitivity," *Optical and Quantum Electronics,* vol. 55, no. 13, p. 1126, 2023.

[64] R. Yahiaoui, A. C. Strikwerda, and P. U. Jepsen, "Terahertz plasmonic structure with enhanced sensing capabilities," *IEEE Sensors Journal,* vol. 16, no. 8, pp. 2484-2488, 2016.

[65] Q. Niu, R. Zhang, and Y. Yang, "High sensitivity and label-free detection of the SARS-CoV-2 S1 protein using a terahertz meta-biosensor," *Frontiers in Physics,* vol. 10, p. 859924, 2022.

Acknowledgment

The authors would like to greatly appreciate Prof. Dr. Hamid Latifi for his help and support.

Author contributions

Seyyedeh Maryam Hosseini proposed the concept, performed the numerical simulation, analyzed the data, and prepared the manuscript. Fazel Jahangiri supervised the project, discussed the results thoroughly, reviewed, and edited the manuscript.

Disclosures

The authors declare no conflicts of interest.

Funding

This research did not receive funding.